J|A|C|S
ARTICLES
Published on Web 11/26/2003

Application of Isomorphous Replacement in the Structure Determination of a Cubic Liquid Crystal Phase and Location of Counterions

Daniel R. Dukeson,[†] Goran Ungar,*[,†] Venkatachalapathy S. K. Balagurusamy,[†] Virgil Percec,[‡] Gary A. Johansson,[‡] and Martin Glodde[‡]

Contribution from the Department of Engineering Materials, University of Sheffield, Sheffield S1 3JD, United Kingdom, and Roy & Diana Vagelos Laboratories, Department of Chemistry, University of Pennsylvania, Philadelphia, Pennsylvania 19104-6323

Received July 18, 2003; E-mail: G.Ungar@Sheffield.ac.uk

Abstract: A second generation monodendron with dodecyl end-groups based on the AB_3 monomer 3,4,5-trihydroxy benzoate has previously been shown to form a thermotropic cubic phase with $Pm\bar{3}n$ symmetry (Balagurusamy et al., *J. Am. Chem. Soc.* **1997**, *119*, 1539). A structure consisting of spherical "micelles" was proposed originally, but an alternative choice of structure factor phases, giving a structure of interlocked squashed columns, could not be ruled out by diffraction data on the original material alone. We have therefore synthesized two selectively fluorinated equivalent compounds, the carboxylic acid and its Rb salt, to be able to apply a variant of the isomorphous replacement crystallographic technique. On the basis of the electron density maps of the new labeled compounds, reconstructed using small-angle X-ray diffraction intensities, the interlocking columns model is unequivocally rejected and the spheres model is upheld. Furthermore, the location of the metal cation in the center of the "micelles" is directly confirmed. Micellar diameter was shown to decrease on fluorination of the dodecyl chain ends, and increase significantly on introduction of Rb. This is interpreted in terms of changes in the number of wedge-shaped dendrons fitting into a spherical micelle due to their changing taper angle. It was found that the Rb-rich regions at the centers of six out of eight "micelles" in the unit cell are elongated in the direction of their closest packing. This adds support to the suggestion of a partial "column-like" character of stacked rows of such micelles, consistent with the position of the $Pm\bar{3}n$ phase next to the columnar phase in the phase sequence of most taper-shape compounds. The results illustrate the potential of isomorphous replacement, used a great deal in protein crystallography, in structure investigation of liquid crystals and supramolecular soft matter.

Introduction

Once the unit cell and the space group are determined, the main task of the crystallographer is to solve the "phase problem", i.e., determine the correct phase angle of the structure factor associated with each X-ray reflection. We can only measure the intensity of a reflection, which is proportional to the square of the amplitude, but cannot measure the phase relationship between waves contributing to different reflections. If we could, this would allow a straightforward and unequivocal determination of electron density distribution in the unit cell, i.e., the structure. Instead, the phase angles must be inferred and compared with other available information on physical viability of a given solution. In classical crystallography there is much additional chemical and physical information available: we know that in a crystal the electron density must be composed of nearly spherical maxima—the atoms. We also know the number and type of atoms (heights of the maxima) in the unit cell, their possible neighboring atoms, approximate interatomic distances, etc. In liquid crystals, individual atoms have no preferred positions and electron density maxima and minima are associated with larger domains populated preferentially by e.g., aromatic or aliphatic moieties, solvent, etc. There is no a priori knowledge of the shape and size of these domains, making the crystallographer's conclusions more ambiguous.

Several years ago,[1,2] we carried out structural analysis of the then newly observed thermotropic cubic phase in a series of monodendron compounds with dodecyl end-groups based on the AB_3 monomer 3,4,5-trihydroxy benzoate. The second generation monodendron, referred to as **$(3,4,5)^2$12G2-CO_2H**, is shown in Scheme 1. The liquid crystal phase has since been observed in many thermotropic dendritic and other amphiphilic systems.[3−12] Its space-group symmetry is $Pm\bar{3}n$, and the

[†] Department of Engineering Materials, University of Sheffield.
[‡] Roy & Diana Vagelos Laboratories, Department of Chemistry, University of Pennsylvania.

(1) Balagurusamy, V. S. K.; Ungar, G.; Percec, V.; Johansson, G. *J. Am. Chem. Soc.* **1997**, *119*, 1539−1555.
(2) Hudson, S. D.; Jung, H.-T.; Percec, V.; Cho, W.-D.; Johansson, G.; Ungar, G.; Balagurusamy, V. S. K. *Science* **1997**, *278*, 449−452.
(3) Borisch, K.; Diele, S.; Göring, P.; Kresse, H.; Tschierske, C. *Angew. Chem., Int. Ed. Engl.* **1997**, *36*, 2087−2089.
(4) Borisch, K.; Diele, S.; Göring, P.; Müller, H.; Tschierske, C. *Liquid Crystals* **1997**, *22*, 427−443.
(5) Percec, V.; Ahn, C.-H.; Ungar, G.; Yeardley, D. J. P.; Moller, M.; Sheiko, S. S. *Nature* **1998**, *391*, 161−164.
(6) Percec, V.; Cho, W.-D.; Mosier, P. E.; Ungar, G.; Yeardley, D. J. P. *J. Am. Chem. Soc.* **1998**, *120*, 11 061−11 070.

10.1021/ja037380j CCC: $25.00

Scheme 1. Structure of **(3,4,5)^{2}12G2-CO$_2$H**.

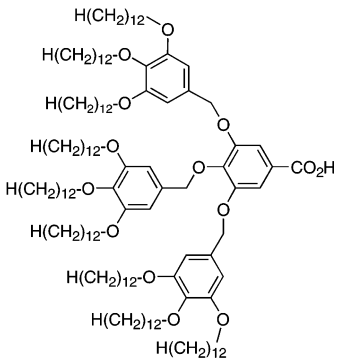

(3,4,5)^{2}12G2-CO$_2$H

proposed structure is shown in Figure 1b. According to this structure, the unit cell contains eight nearly spherical electron density maxima of similar size, one at the corners of the cubic cell, one in the body center, and six on lines bisecting each face. This structure is similar to the one with the same spacegroup symmetry found in some normal lyotropic (lipid−water) micellar liquid crystals, where polar groups are on the surface of the spheres, facing water, and the paraffinic chains are inside.[13] By contrast, the molecular arrangement proposed for the thermotropic $Pm\bar{3}n$ phase in dendrons has the aliphatic chains outside the spheres, with the aromatic dendritic cores inside.

Despite the attractiveness of the spheres model of the thermotropic $Pm\bar{3}n$ phase, there is an alternative model obtained by making a different choice of structure factor phase angles. Because the space group is centrosymmetric, the phase angles are limited to 0° or 180°, i.e., to the positive or negative sign of each structure factor. Reconstructed using only the three strongest X-ray reflection groups, {200}, {210}, and {211}, the isosurface of the alternative $Pm\bar{3}n$ structure is shown in Figure 1a. It consists of interlocking squashed columns stretching along the three principal directions [100], [010], and [001].

For the thermotropic $Pm\bar{3}n$ phase, the evidence based on electron density histograms[1] and electron microscopy[2] weighs toward the spherical model. Moreover, since the discovery of this phase, two additional phases with spherical aggregates were found in thermotropic systems, both self-assembled from tapered dendron molecules: a body-centered cubic (space group $Im\bar{3}m$),[14] and a complex tetragonal (spacegroup $P4_2/mnm$).[15] Despite this,

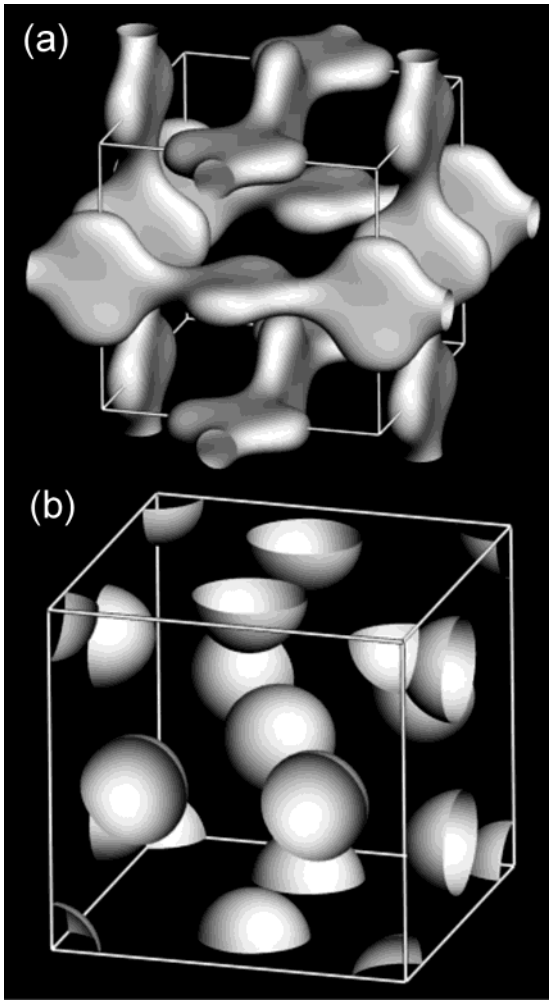

Figure 1. Two alternative structures of the $Pm\bar{3}n$ cubic liquid crystal unit cell in thermotropic supramolecular dendrimer **(3,4,5)^{2}12G2-CO$_2$H**. The isoelectron surface (surface connecting points of equal electron density) is shown, as reconstructed from X-ray diffraction data. The isosurface divides the volume into the high-density 20 vol % (enclosed, aromatic) and the low-density 80 vol % (continuum, aliphatic).

the interlocking columns model of the $Pm\bar{3}n$ phase cannot be discarded. It has been noted that, as the molecular taper angle is increased, e.g., by increasing the temperature, the sequence of phases is as follows: hexagonal columnar → $Pm\bar{3}n$ → $P4_2/mnm$ → $Im\bar{3}m$.[15] Thus, the $Pm\bar{3}n$ phase is on the borderline between columnar and spherical self-assembly; hence, the interlocking columns model would not be out of line. Furthermore, several different artificially created interlocking bar structures have been shown to present highly efficient photonic band gap crystals,[16] and it would be of considerable interest to find if a similar structure is created by molecular self-assembly. For these reasons, and for the fact that $Pm\bar{3}n$ is the most abundant phase in highly tapered mesogens, it is important that its exact structure is established with greater certainty.

To achieve this, we apply here the crystallographic technique of isomorphous replacement. This method is commonly used in protein crystallography, where a strongly scattering heavy metal marker is attached to a specific known position in the protein molecule, without altering the crystal structure.[17] It was found by Perutz[18] and Kendrew[19] that, due to its large number

(7) Cheng, X. H.; Diele, S.; Tschierske, C. *Angew. Chem., Int. Ed.* **2000**, *39*, 592−595.
(8) Percec, V.; Cho, W.-D.; Ungar, G.; Yeardley, D. J. P. *Angew. Chem., Int. Ed.* **2000**, *39*, 1597−1602.
(9) Ungar, G.; Percec, V.; Holerca, M. N.; Johansson, G.; Heck, J. A. *Chem. Eur. J.* **2000**, *6*, 1258−1266.
(10) Borisch, K.; Tschierske, C.; Göring, P.; Diele, S. *Langmuir* **2000**, *16*, 6701−6708.
(11) Percec, V.; Cho, W.-D.; Ungar, G.; Yeardley, D. J. P. *J. Am. Chem. Soc.* **2001**, *123*, 1302−1315.
(12) Percec, V.; Holerca, M. N.; Uchida, S.; Cho, W.-D.; Ungar, G.; Lee, Y. S.; Yeardley, D. J. P. *Chem. Eur. J.* **2002**, *8*, 1106−1117.
(13) (a) Fontell, K.; Fox, K. K.; Hansson, E. *Mol. Cryst. Liq. Cryst., Lett.* **1985**, *1*, 9−17. (b) Charvolin, J.; Sadoc, J. F. *J. Phys., Paris* **1988**, *49*, 521−526. (c) Vargas, R.; Mariani, P.; Gulik, A.; Luzzati, V. *J. Mol. Biol.* **1992**, *225*, 137−145. (d) Luzzati, V.; Vargas, R.; Mariani, P.; Gulik, A.; Delacroix, H. *J. Mol. Biol.* **1993**, *229*, 540−551.
(14) (a) Yeardley, D. J. P.; Ungar, G.; Percec, V.; Holerca, M. N.; Johansson, G. *J. Am. Chem. Soc.* **2000**, *122*, 1684−1689. (b) Duan, H.; Hudson, S. D.; Ungar, G.; Holerca, M. N.; Percec, V. *Chem. Eur. J* **2001**, *7*, 4134−4141.
(15) Ungar, G.; Liu, Y.; Zeng, X. B.; Percec, V.; Cho, W.-D. *Science* **2003**, *299*, 1208−1211.
(16) *Photonic Band Gap Materials*; Soukoulis C. M., Ed.; Kluwer Academic Publishers: London, 1996

Scheme 2. Synthesis of **(3,4,5)²12F8G2-CO₂H**[a]

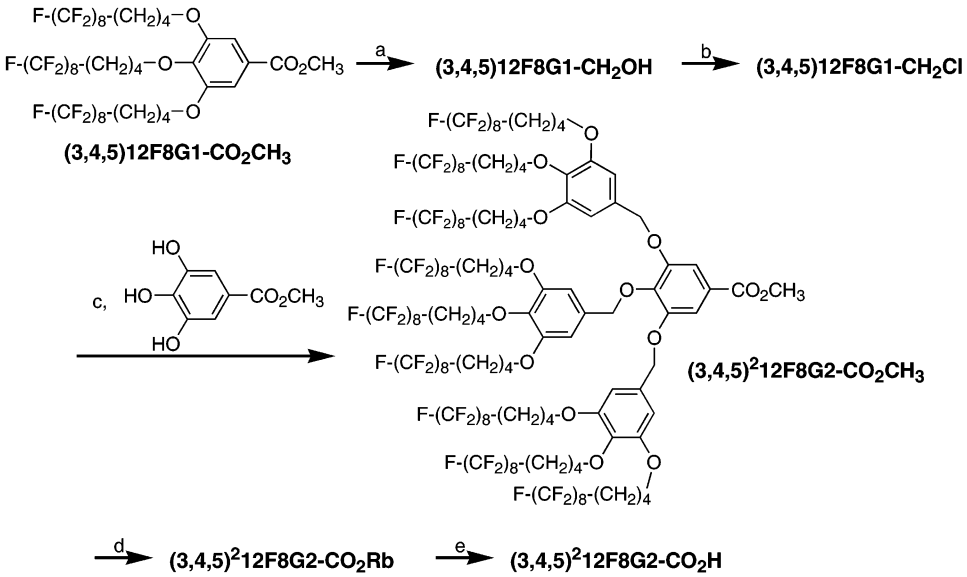

[a] (a) $LiAlH_4$, Et_2O, 22 °C, then NaOH, H_2O, 88%; (b) $SOCl_2$, α,α,α-trifluorotoluene, 22 °C, 70%; (c) DMF/α,α,α-trifluorotoluene, K_2CO_3, 70 °C, then Freon 113, 18-C-6, 48 °C, 65%; (d) RbOH, THF, EtOH, 20 h, 65 °C, 90%; (e) CH_3CO_2H, Freon 113, 25 °C, 10 min, 66%.

of electrons, the addition of only one such atom per molecule can produce a notable effect on the diffraction pattern of the protein crystal. This effect can be utilized for initial phasing of the reflections. The method of isomorphous replacement has led initially to the structure determination of myoglobin[19] and hemoglobin,[18] and has opened the way for the current proliferation of some 2000 new protein structures annually.[20]

Although the problems of structure determination in nanoscale supramolecular self-assembled and liquid crystal systems are quite different from those in proteins, the lack of firm a priori information which would constrain the phase choice is one aspect they share. In the present work, we use two kinds of marking by electron-rich species: (a) selective perfluorination of outer portions of the aliphatic chains, and (b) partial replacement of carboxylic hydrogen with rubidium. To our knowledge, this is the first application of isomorphous replacement technique in liquid crystals and self-assembled nanostructures.

Results and Discussion

Synthesis of (3,4,5)²12F8G2-CO₂H and (3,4,5)²12F8G2-CO₂Rb. Scheme 2 outlines the synthesis of the second generation (G2) semi-fluorinated monodendrons based on the AB_3 monomer 3,4,5-trihydroxy benzoate, i.e., **(3,4,5)²12F8G2-CO₂R**, where (3,4,5−3,4,5) or $(3,4,5)^2$ indicates a 3,4,5-substitution pattern in each generation of the AB_3 building blocks, 12F8 denotes a C_{12} alkyl chain containing $(CF_2)_8F$ end groups, and CO_2R is the carboxylic group (salt or acid) at the apex of the monodendron. The synthesis of **(3,4,5)²12F8G2-CO₂Me** was reported elsewhere.[21] The corresponding Rb salt i.e., **(3,4,5)²12F8G2-CO₂Rb**, was prepared by saponification of **(3,4,5)²12F8G2-CO₂CH₃** with RbOH in a mixture of THF and ethanol. The resulting Rb salt was soluble in Freon 113. Therefore, the acid **(3,4,5)²12F8G2-CO₂H** was prepared from its Rb salt by addition of glacial acetic acid to a Freon 113 solution of the salt.

Thermal Analysis. The phase behavior of the monodendrons **(3,4,5)²12F8G2-CO₂R** was determined by a combination of thermal optical polarized microscopy and differential scanning calorimetry (DSC). The phases were assigned by X-ray analysis as discussed in detail in the next section.

All compounds of generation G2 decompose at about 250 °C. Whereas the acid **(3,4,5)²12F8G2-CO₂H** exhibits the cubic−isotropic liquid transition, the corresponding Rb salt decomposes before isotropization. Mixtures of **(3,4,5)²12F8G2-CO₂Rb** with the corresponding acid **(3,4,5)²12F8G2-CO₂H** of up to 60 mol-% Rb salt content exhibit isotropization temperatures below 250 °C as shown in Figure 2. This allowed us to perform X-ray studies of these mixtures.

X-ray Analysis. Figure 3 shows the small-angle X-ray diffraction curves of unoriented samples of the nonfluorinated acid **(3,4,5)²12G2-CO₂H**, fluorinated acid **(3,4,5)²12F8G2-CO₂H** and the 4:1 molar mixture of **(3,4,5)²12F8G2-CO₂H and (3,4,5)²12F8G2-CO₂Rb**, denoted **(3,4,5)²12F8G2-CO₂H$_{0.8}$Rb$_{0.2}$**. The appearance of the diffractograms of the fluorinated dendrons differs considerably from that of **(3,4,5)²12G2-CO₂H**, primarily by the presence of strong reflections at higher angles. Nevertheless, after numerical curve resolution, all observed reflections could be indexed on a cubic lattice, as shown in Table 1. The observed reflections satisfy the conditions for space group $Pm\bar{3}n$, i.e., 00h: h is even and hhl: l is even.

The lattice parameter *a* is 63.9 Å for **(3,4,5)²12F8G2-CO₂H** and 79.0 Å for **(3,4,5)²12F8G2-CO₂H$_{0.8}$Rb$_{0.2}$**. For the original

(17) *Practical Protein Crystallography*; McRee, D. E.; Academic Press: San Diego, 1993; p 131.
(18) Perutz, M. F.; Rossman, M. G.; Cullis, A. F.; Muirhead, H.; Will, G.; North, A. C. T. *Nature* **1960**, *185*, 416−421.
(19) Kendrew, J. C.; Bodo, G.; Dintzis, H. M.; Parrish, R. G.; Wyckoff, H. W.; Phillips, D. C. *Nature* **1958**, *181*, 662−666.
(20) Thomas, J. M. *Angew. Chem., Int. Ed.* **2002**, *41*, 3155−3166.
(21) (a) Percec, V.; Johansson, G.; Ungar, G.; Zhou, J. *J. Am. Chem. Soc.* **1996**, *118*, 9855−9866. (b) Johansson, G.; Percec, V.; Ungar, G.; Zhou, J. *Macromolecules* **1996**, *29*, 646−660. (c) Percec, V.; Glodde, M.; Bera, T. K.; Miura, Y.; Shiyanovskaya, I.; Singer, K. D.; Balagurusamy, V. S. K.; Heiney, P. A.; Schnell, I.; Rapp, A.; Spiess, H.-W.; Hudson, S. D.; Duan, H. *Nature* **2002**, *419*, 384−387. (d) Percec, V.; Glodde, M.; Johansson, G.; Balagurusamy, V. S. K.; Heiney, P. A. *Angew. Chem., Int. Ed.* **2003**, *42*, 4338−4342.

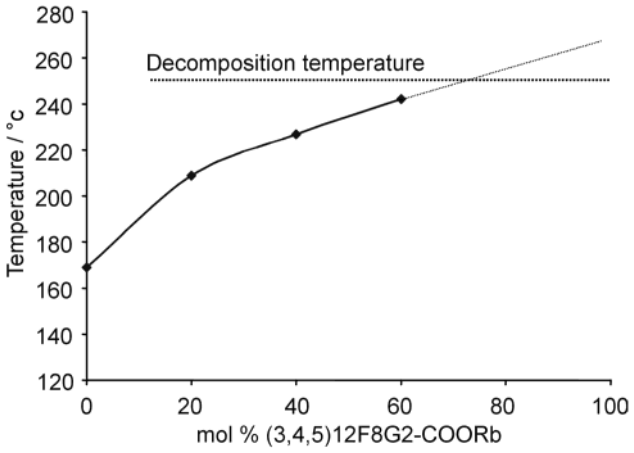

Figure 2. Cubic−isotropic liquid transition temperature vs composition for the **(3,4,5)^{2}12F8G2-CO$_2$H** + **(3,4,5)^{2}12F8G2-CO$_2$Rb** system, determined from the first DSC heating run.

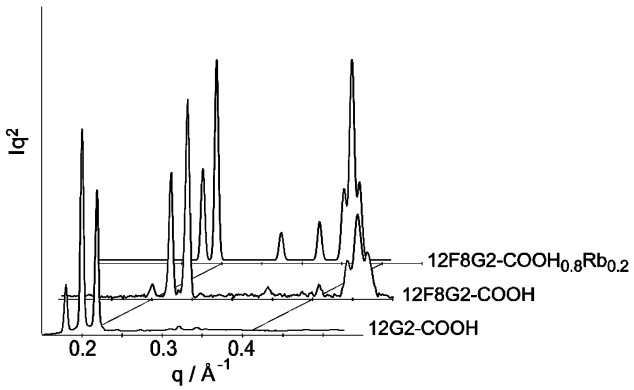

Figure 3. Small-angle X-ray powder diffractograms of the $Pm\bar{3}n$ phase. (front) **(3,4,5)^{2}12G2-CO$_2$H**, (middle) **(3,4,5)^{2}12F8G2-CO$_2$H**, (back) **(3,4,5)^{2}12F8G2-CO$_2$H** + **(3,4,5)^{2}12F8G2-CO$_2$Rb** (80:20). The intensities are Lorentz corrected and normalized to the strongest reflection. $q = 4\pi\sin\theta/\lambda$, where θ is half the scattering angle and λ is the wavelength.

Table 1. X-ray Spacings and Intensities for **(3,4,5)^{2}12F8G2-CO$_2$H** and **(3,4,5)^{2}12F8G2-CO$_2$H$_{0.8}$Rb$_{0.2}$**

	(3,4,5)^{2}12F8G2-CO$_2$H			(3,4,5)^{2}12F8G2-CO$_2$H$_{0.8}$Rb$_{0.2}$		
reflection *hkl*	d_{exp}/Å[a]	d_{calc}/Å	I_{hkl}	d_{exp}/Å[b]	d_{calc}/Å	I_{hkl}
200	31.8	31.9	23			
210	28.4	28.5	56	35.6	35.3	44
211	26.0	26.0	100	32.3	32.3	100
222	18.5	18.4	16	22.9	22.8	43
410	15.5	15.5	5	19.3	19.2	20
420	14.3	14.3	23	17.7	17.7	43
421	13.9	13.9	35	17.2	17.2	67
332	13.6	13.6	40	16.8	16.8	47

[a] Recorded at 117 °C. [b] Recorded at 125 °C.

nonfluorinated **(3,4,5)^{2}12G2-CO$_2$H**, a was 68.3 Å. Fluorinated acid-salt mixtures with salt fraction 0.4 or higher did not display the $Pm\bar{3}n$ phase, hence could not be used for isomorphous replacement experiments.

The electron density distribution, $\rho(\mathbf{r})$, is related to the diffraction amplitude F through[22]

$$\rho(\mathbf{r}) = \frac{1}{V}\sum_{\mathbf{h}_\alpha} q(\mathbf{h}_\alpha)F(\mathbf{h}_\alpha)[A(\mathbf{h}_\alpha) - iB(\mathbf{h}_\alpha)] \qquad (1)$$

(22) *International Tables for Crystallography*; Shmeueli U., Ed.; Kluwer Academic Publishers: Dordrecht, 1996; Vol. B.

where V is the unit cell volume, q is inverse multiplicity, $\mathbf{r}$ and $\mathbf{h}_\alpha$ are the real and reciprocal space vectors, respectively, and A and B are the "geometric structure factors". In cases where a center of symmetry is present, the structure factor is real, i.e., $B = 0$, and for an ordered lattice with discrete *hkl* reflections

$$\rho(xyz) = \frac{2}{V}\sum_{h,k,l} q_{hkl}F_{hkl}A_{hkl} \qquad (2)$$

Here x, y, z are components of $\mathbf{r}$, and h, k, l are Miller indices components of $\mathbf{h}_\alpha$. Although for complex structure factors as in eq 1 the phase can assume any angle between 0 and 2π, for centrosymmetric spacegroups such as $Pm\bar{3}n$ possible phase angles are restricted to 0 or π, i.e., to the positive or negative sign of the structure factor.

The diffractogram of the nonfluorinated **(3,4,5)^{2}12G2-CO$_2$H** is dominated by three reflections (Figure 3), and to a good approximation $\rho(xyz)$ is represented by eq 2 using one of the $2^3 = 8$ phase combinations. In fact, the number of significantly different combinations is halved when an arbitrary choice of origin is allowed for, and halved again if one is not concerned with the sign of $\rho(xyz)$. The two remaining possible solutions are shown in Figure 1.

For fluorinated compounds there are eight reasonably strong reflections in the powder pattern which give $2^8 = 256$ possible phase combinations. In analogy with the above, reducing this to a quarter results in 64 distinct combinations. In the case of **(3,4,5)^{2}12F8G2-CO$_2$H** we have calculated $\rho(xyz)$ for 125 000 volume elements of the unit cell for all 64 phase combinations. These data were used to generate electron density histograms, isoelectron surfaces, and two-dimensional maps.

Spheres vs. Interlocking Columns Model. Crude electron density models were built based on molecular dimensions, representing the interlocking columns and the spheres model. These are then compared against the 64 reconstructed $\rho(xyz)$ functions. The model of the **(3,4,5)^{2}12F8G2-CO$_2$H** molecule is split into segments and the ratio n_e/V_s of the number of electrons and the van der Waals volume of the segment is calculated. It emerges that the molecule can be represented, in a first approximation, by three electron density regions, as represented in Figure 4a. The lowest density (red) region is aliphatic, the medium density (green) region contains the largely aromatic dendritic core, whereas the perfluorinated outer portions of the chains have the highest electron density (blue). Scaling the aliphatic electron density to 1, the densities of the aromatic and the fluorinated regions are 1.6 and 2. In considering the model $\rho(xyz)$, it is assumed that the dendron cores are located near the center of the columns, or spheres, with the fluorinated regions segregated into interstitial spaces.

A systematic search has established that none of the 64 reconstructed $\rho(xyz)$ distributions are compatible with the interlocking columns model in Figure 1a, as applied to **(3,4,5)^{2}12F8G2-CO$_2$H**.

The next stage is to examine whether a solution could be found which is compatible with the spheres model. If so, the third stage would be to test the validity of the phase choice by applying the same phase combination in calculating $\rho(xyz)$ for

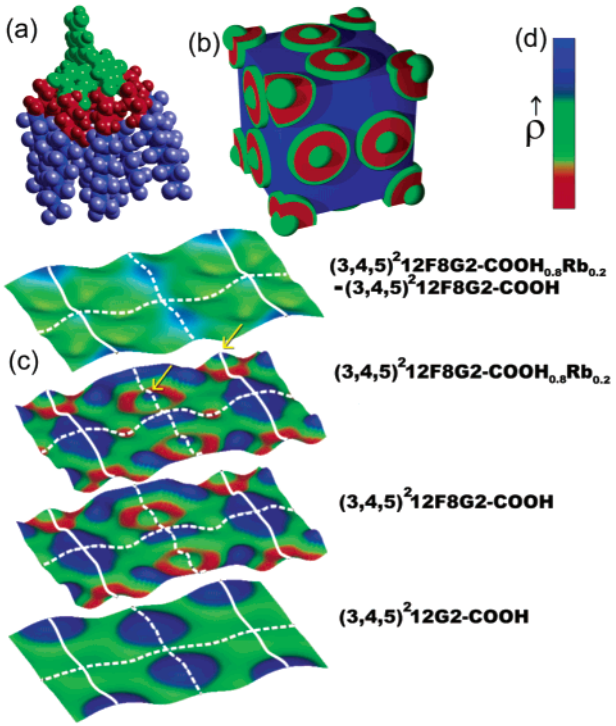

Figure 4. Expected and observed electron density (ρ) distributions. (a) Molecular model of **(3,4,5)²12F8G2-CO_2H** with the lowest ρ aliphatic portions in red, the medium ρ, predominantly aromatic core in green, and the highest ρ fluorinated portions in blue. (b) Expected $\rho(x,y,z)$ distribution in a $Pm\bar{3}n$ unit cell of **(3,4,5)²12F8G2-CO_2H** according to the spheres model. (c) 2-Dimensional $\rho(x,y)$ maps of the $z = 0$ level for **(3,4,5)²12G2-CO_2H** (bottom), **(3,4,5)²12F8G2-CO_2H** (second from bottom) and **(3,4,5)²12F8G2-$CO_2H_{0.8}Rb_{0.2}$** (second from top). Top is a difference map of **(3,4,5)²12F8G2-$CO_2H_{0.8}Rb_{0.2}$**−**(3,4,5)²12F8G2-CO_2H**. 1.5 unit cells are shown; full lines delimit a cell, dashed lines are cell bisectors. The maps were reconstructed using eq 2 with the phase combinations given in Table 2. Note that the only difference between the maps for fluorinated acid and its Rb salt is the increased height of the center-of-sphere peaks in the latter map (marked by arrows). (d) Color coding.

(3,4,5)²12F8G2-$CO_2H_{0.8}Rb_{0.2}$, and observe if an increase in ρ occurred at the expected Rb locations.

Figure 4b shows schematically the anticipated color-coded electron density distribution in a unit cell for the spheres model of **(3,4,5)²12F8G2-CO_2H**. Note that an expected medium-density transition domain (green) is interposed between each minimum density aliphatic and maximum density fluorinated region. Inspection of the reconstructed $\rho(xyz)$ distributions has shown that two of them come close to that expected, the closer being the one represented by the 2-dimensional map of the $z = 0$ level in Figure 4c (second from bottom). Green maxima, indicating the centers of the "micelles" are seen at the corners of the unit cell (0,0,0) as well as on the central bisector ($^1/_2$,$^1/_4$,0 and $^1/_2$, $^3/_4$, 0). These are surrounded by red "moats" associated with the aliphatic region. The highest density (blue) regions are indeed at the predicted outermost positions, although they do not provide as smooth a continuum as might be expected from the idealized model in Figure 4b. The map for **(3,4,5)²12F-8G2-CO_2H** should be compared with that for **(3,4,5)²12G2-CO_2H** at the bottom of Figure 4c. The latter contains only two types of regions, the higher density aromatic (blue) at the centers of the supramolecular dendrimer "micelles", and the lower density aliphatic (green) regions elsewhere.

Electron density histograms are a tool used for initial screening of the different structure factor phase combinations. The histograms give the volume fractions of the different electron density levels within a unit cell. This method was used in previous studies on nonfluorinated dendrons,[1,14b,15] where the correct structure gave a bimodal, albeit smeared, distributiondue to microphase separation between aromatic and aliphatic moieties. In the present case, the expected idealized distribution is trimodal (aliphatic, aromatic, fluorinated), and the calculated histogram for the phase combination represented by ρ (xyz) in Figure 4a indeed shows a smeared trimodal distribution (see Supplementary Information).

Location of Rb^+ Ions. Replacing 20% of carboxylic hydrogen with Rb is expected to increase ρ in the middle of the "aromatic" core of the micelles. This moderate increase in the total number of electrons in the core is not likely to change the phase of any of the structure factors and could thus be used to additionally test the phase choice for **(3,4,5)²12F8G2-CO_2H**. The reconstructed $\rho(xyz)$ for **(3,4,5)²12F8G2-$CO_2H_{0.8}Rb_{0.2}$** is included as a $z = 0$ level map in Figure 4c (second from top). The map indeed shows the change expected: compared with the map for **(3,4,5)²12F8G2-CO_2H**, the peaks at micelle centers had become higher (marked by arrows). There is otherwise very little noticeable change to the map. This result gives further support for the phase combination selected, and hence for the spheres model of the $Pm\bar{3}n$ phase. In addition, it confirms that it is indeed possible to use self-assembly to place specific chemical entities such as metal ions on selected positions in a liquid crystal lattice, in this instance, encapsulating them in spherical nano-objects.

To pinpoint the rubidium ions we have subtracted the electron density map of **(3,4,5)²12F8G2-CO_2H** from that of **(3,4,5)²-12F8G2-$CO_2H_{0.8}Rb_{0.2}$**—see the top map in Figure 4c. As expected, the maxima (blue) in this $\Delta\rho(xy)$ difference map are located at the centers of the "micelles". It is informative to examine the 3-dimensional difference map $\Delta\rho(x,y,z)$, which is shown in Figure 5. The isosurface encloses the regions of highest $\Delta\rho$, i.e., the regions containing rubidium. The eight "micelles" in the $Pm\bar{3}n$ phase occupy two crystallographically nonequivalent symmetry (Wyckoff) positions;[22] those at the corners and at the center of the unit cell (positions *a*) are different from those on the bisectors of the cell faces (positions *c*). In Figure 5 the Rb domains at the core of "*a*-micelles" have a somewhat distorted spherical shape (octahedral distortion), while the cores of "*c*-micelles" are elongated along the bisector lines (dashed lines in Figure 5).

The elongated shape of the *c*-type Rb zones is in fact consistent with our recently proposed model of molecular arrangement in the $Pm\bar{3}n$ phase.[15] It can be shown that the *c*-micelles in this phase are in exceptionally close contact along the rows defined by the face bisectors (Figure 6a,d). The tetrakaidecahedra, which are the Wigner−Seitz cells delimiting the *c*-micelles,[23] are squashed in their stacking direction (Figure 6a). This implies a degree of preferred molecular orientation in the equatorial plane of the micelles (Figure 6c), and hence an elongation of the −COOH domains along the stacking direction. A much higher degree of equatorial orientation is, of course, achieved in the columnar phase (Figure 6b), which many $Pm\bar{3}n$ liquid crystals display at lower temperatures.[9,11,12] If such anisotropic *c*-micelles contain rubidium at their core, the Rb zone is expected to be extended meridionally, as schematically

(23) Charvolin J.; Sadoc J. F. *J. Phys. (France)* **1988**, *49*, 521−526.

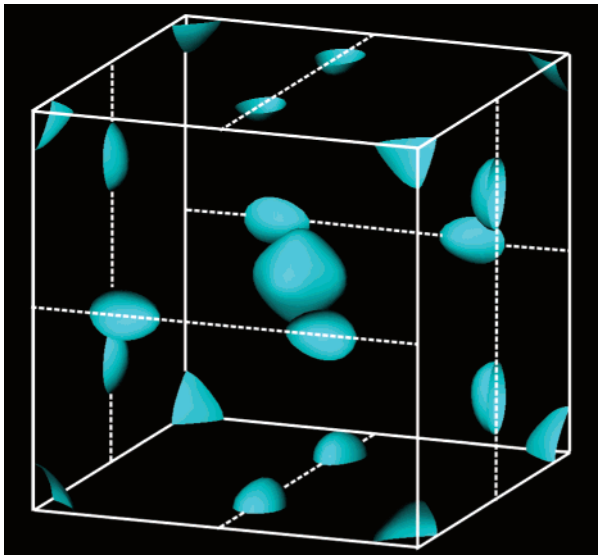

Figure 5. 3-dimensional electron density difference map. Isoelectron surface encloses the high-density regions of the map of the **(3,4,5)^{2}12F8G2-CO$_2$H$_{0.8}$Rb$_{0.2}$** unit cell from which the **(3,4,5)^{2}12F8G2-CO$_2$H** map had been subtracted. Thus, the enclosed regions contain Rb ions. The Rb regions at Wyckoff positions *c* are elongated along the face bisectors.

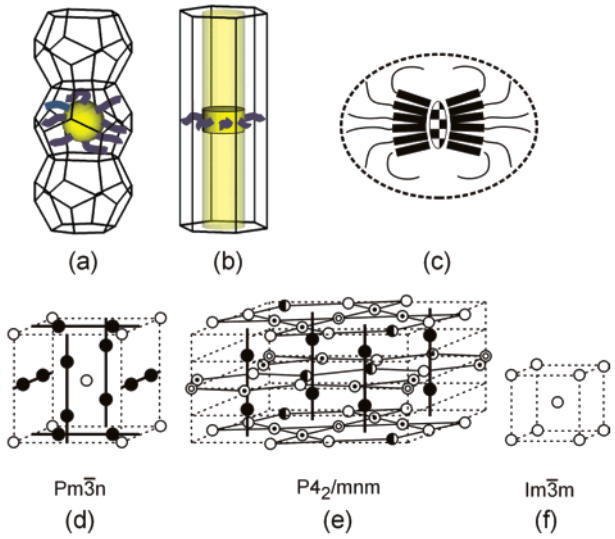

Figure 6. Self-assembly of dendrons in different mesophases. (a) Stacking of space-filling polyhedra delimiting individual "*c*-micelles" along the solid lines in (d). (b) A column in the columnar phase considered as a stack of merged micelles. (c) Proposed molecular arrangement within a "*c*-micelle" of **(3,4,5)^{2}12F8G2-CO$_2$H$_{0.8}$Rb$_{0.2}$** (side view). Thick lines denote the aromatic cores viewed edge-on, thin lines the flexible tails and the checkered area is the location of the Rb. (d,e,f) Unit cells of the three "micellar" phases. Micelles of the same symmetry are shown with the same symbol. Close contacts are shown by solid lines (after ref 15).

shown in Figure 6c. Thus, the elongated shape of Rb domains at *c* positions (Figure 5) is consistent with the "squashed micelle" concept. It should be noted that, even though a micelle may contain only a couple of Rb ions (see below), due to their delocalization in the liquid crystal, X-ray diffraction gives the average distribution of such ions in space and time.

While 6 out of 8 micelles (75%) in the *Pm*$\bar{3}$*n* phase have close contacts (Figure 6d), only 8 out of 30 micelles (27%) have close contacts in the recently discovered tetragonal *P*4$_2$/*mnm* phase (Figure 6e), whereas there are no close contacts in the body-centered *Im*$\bar{3}$*m* phase (Figure 6f).[15] There is clear correlation between the proportion of close contacts and the

Table 2. Phase Combinations Used for the Construction of Electron Density Maps in Figure 4 and Figure 5

compd	phase combination
(3,4,5)^{2}12G2-CO$_2$H	+(200),−(210),+(211)
(3,4,5)^{2}12F8G2-CO$_2$H	−(200), +(210), −(211), +(222), −(410), +(420), −(421), +(332)
(3,4,5)^{2}12F8G2-CO$_2$H$_{0.8}$Rb$_{0.2}$	+(210), −(211), +(222), −(410), +(420), −(421), +(332)

Table 3. Number of Dendrons Per Spherical Supramolecular Dendrimer

dendron	*T* (°C)	unit cell parameter, *a* (Å)	density (g·cm^{-3})[a]	M.W. (daltons)	average no. of molecules per "micelle",[b] μ	v.d.W. volume,[c] *v* (Å^3)	packing fraction[d]
(3,4,5)^{2}12G2-CO$_2$H	105	68.3	0.99	2057	**11.3**	2250	0.64
(3,4,5)^{2}12F8G2-CO$_2$H	117	63.9	1.70	4810	**6.9**	2962	0.63
(3,4,5)^{2}12F8G2-CO$_2$H$_{0.8}$Rb$_{0.2}$	125	79.0	1.70	4827	**12.8**	3028	0.63

[a] Experimental, at 22 °C. [b] (Number of molecules per unit cell)/8. [c] Volume enclosed by van der Waals surface of a molecule, calculated using Cerius-2. [d] $8\mu v/a^3$.

sequence of phases with increasing temperature in alkyl-terminated self-assembled dendrimers, viz. hexagonal columnar → *Pm*$\bar{3}$*n* → *P*4$_2$/*mnm* → *Im*$\bar{3}$*m*.[9,11,12] This sequence coincides with a decreasing fraction of close micellar contacts and the progressive loss of columnar character. The sequence is in line with increasing lateral expansion of the alkyl tails and the dendrons becoming more cone-shaped and less slice-shaped.

Variation in Micellar Size. Finally, we consider the effect of fluorination and the introduction of Rb on the size of the micelles and of the unit cell. Fluorination reduces the cubic lattice parameter *a* from 68.3 Å for **(3,4,5)^{2}12G2-CO$_2$H** to 63.9 Å for **(3,4,5)^{2}12F8G2-CO$_2$H**, a volume decrease of 22%. At the same time, the substitution of 20% of carboxylic hydrogen by Rb increases *a* to 79.0 Å, a volume increase of 89%. The differences in molecular volume between these compounds are relatively minor, as shown in Table 3. This implies that the variations in unit cell volume are primarily due to differences in the number of molecules per cell and, accordingly, per "micelle"—see Table 3, sixth column.

Packing of conical dendrons into spheres is illustrated schematically in Figure 7. A tapered molecule is characterized by its solid angle α, and the optimum number of molecules per sphere is given by $\mu = 4\pi/\alpha$. Fluorination increases the pendant chain cross-section and thus increases α, thereby decreasing μ (Figure 7c and Table 3). On the other hand, the introduction of Rb ions at the center of the sphere shifts the dendrons away from the center. This increases the number of dendrons, μ, required to complete the sphere. However, addition of extra dendron anions in turn requires the addition of more Rb, etc. The final equilibrium is reached after a near doubling in μ (Table 3 and Figure 7d). Thus a small volume addition at the center of the "micelle" (see Table 3, 7th column) causes a disproportionately large increase in micellar volume. A similar argument has been applied to explain the drastic effect of cation size on the cubic unit cell size of alkali salts of **(3,4,5)G1-CO$_2$H**, the first generation dendron equivalent of **(3,4,5)^{2}12G2-CO$_2$H**.[9]

Considering that the materials are liquid crystalline, our interpretation of the fact that such odd numbers of molecules pack in a sphere is as follows. (a) The number is an average

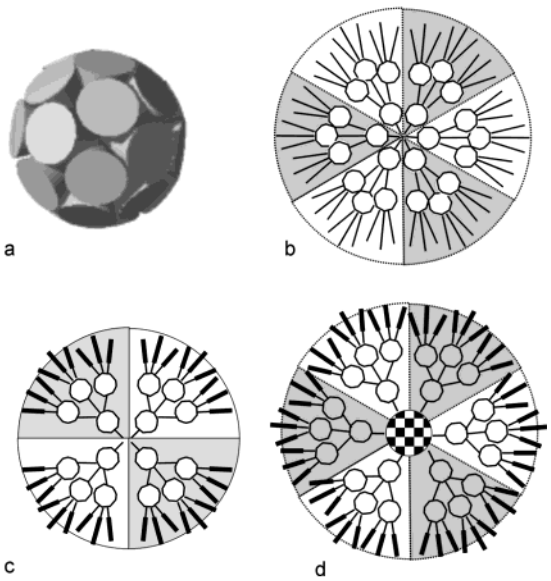

Figure 7. (a) Schematic representation of the packing of conical dendrons in a spherical supramolecular dendrimer. (b), (c), (d) two-dimensional representation for **(3,4,5)^{2}12G2-CO$_2$H, (3,4,5)^{2}12F8G2-CO$_2$H** and **(3,4,5)^2-12F8G2-CO$_2$H$_{0.8}$Rb$_{0.2}$**, respectively. The checkered circle in (d) symbolizes the area populated by Rb.

over space and time, and (b) the dendron shape is adaptable with the preservation of incompressibility (uniform space filling) being a high priority. Similarly, the small fractional number of Rb ions per micelle ($0.2 \times 12.8 = 2.5$) for **(3,4,5)^{2}12F8G2-CO$_2$H** and **(3,4,5)^{2}12F8G2-CO$_2$H$_{0.8}$Rb$_{0.2}$**, refers to the average micelle.

Conclusion

The interlocked columns model was rejected as a possible structure of the $Pm\bar{3}n$ phase, confirming earlier work suggesting the discrete micelle model. Location of cations at the micellar centers is confirmed directly. The reduction in micellar size through fluorination, and the increase through introduction of Rb^+, is explained by variation in the number of dendrons per micelle, caused by changes in molecular taper angle. The elongated rather than spherical shape of Rb-rich regions at the centers of the six micelles on face bisectors provides further support for the proposed anisotropic character of these micelles forming rows of close contacts. This in turn is consistent with the $Pm\bar{3}n$ micellar phase being closest to the columnar phase in the thermotropic sequence of currently known phases.

We have shown here that the isomorphous replacement method may be applied successfully in resolving basic as well as detailed features of liquid crystal and supramolecular structures. It is our view that, if supramolecular chemistry is to advance further and produce ever more complex structures, there needs to be a parallel continuing advance in rigorous structural characterization techniques, as has happened in the field of structural biology.

Acknowledgment. Financial support by Engineering and Physical Science Research Council (EPSRC) and the National Science Foundation (NSF) is gratefully acknowledged. We thank A. J. Gleeson for help in setting up the SAXS experiment, and Professor S. Z. D. Cheng for density measurements.

Supporting Information Available: Experimental section and explanation of structure factor phase combination selection (PDF). This material is available free of charge via the Internet at http://pubs.acs.org.

JA037380J